Cobatoxin 1 from *Centruroides noxius* scorpion venom: chemical synthesis, three-dimensional structure in solution, pharmacology and docking on K$^+$ channels

Besma JOUIROU*†[1], Amor MOSBAH*[1], Violeta VISAN‡, Stephan GRISSMER‡, Sarrah M'BAREK*, Ziad FAJLOUN*, Jurphaas VAN RIETSCHOTEN*, Christiane DEVAUX*, Hervé ROCHAT*, Guy LIPPENS§, Mohamed EL AYEB*†, Michel DE WAARD¶, Kamel MABROUK* and Jean-Marc SABATIER*[2]

*Laboratoire International Associé d'Ingénierie Biomoléculaire, CNRS UMR 6560, Bd Pierre Dramard, 13916 Marseille Cedex 20, France, †Laboratoire des Venins et Toxines, Institut Pasteur de Tunis, Tunis-Belvédère, Tunisia, ‡Universität Ulm, Albert Einstein-Allee 11, D-89081 Ulm, Germany, §CNRS UMR 8525, Institut Pasteur de Lille, 1 rue du Professeur Calmette BP447, 59021, Lille Cedex, France, and ¶Inserm EMI 9931, CEA, IFR 27, DRDC, Canaux Ioniques et Signalisation, 17 rue des Martyrs, 38054 Grenoble Cedex 09, France

CoTX1 (cobatoxin 1) is a 32-residue toxin with three disulphide bridges that has been isolated from the venom of the Mexican scorpion *Centruroides noxius* Hoffmann. Here we report the chemical synthesis, disulphide bridge organization, 3-D (three-dimensional) solution structure determination, pharmacology on K$^+$ channel subtypes (voltage-gated and Ca^{2+}-activated) and docking-simulation experiments. An enzyme-based cleavage of the synthetic folded/oxidized CoTX1 indicated half-cystine pairs between Cys^3-Cys^{22}, Cys^8-Cys^{27} and Cys^{12}-Cys^{29}. The 3-D structure of CoTX1 (solved by ^{1}H-NMR) showed that it folds according to the common α/β scaffold of scorpion toxins. *In vivo*, CoTX1 was lethal after intracerebroventricular injection to mice (LD$_{50}$ value of 0.5 μg/mouse). *In vitro*, CoTX1 tested on cells expressing various voltage-gated or Ca^{2+}-activated (IKCa1) K$^+$ channels showed potent inhibition of currents from rat K$_v$1.2 (K_d value of 27 nM). CoTX1 also weakly competed with ^{125}I-labelled apamin for binding to SKCa channels (small-conductance

Ca^{2+}-activated K$^+$ channels) on rat brain synaptosomes (IC$_{50}$ value of 7.2 μM). The 3-D structure of CoTX1 was used in docking experiments which suggests a key role of Arg^6 or Lys^{10}, Arg^{14}, Arg^{18}, Lys^{21} (dyad), Ile^{23}, Asn^{24}, Lys^{28} and Tyr^{30} (dyad) residues of CoTX1 in its interaction with the rat K$_v$1.2 channel. In addition, a [Pro^7,Gln^9]-CoTX1 analogue (ACoTX1) was synthesized. The two residue replacements were selected aiming to restore the RPCQ motif in order to increase peptide affinity towards SKCa channels, and to alter the CoTX1 dipole moment such that it is expected to decrease peptide activity on K$_v$ channels. Unexpectedly, ACoTX1 exhibited an activity similar to that of CoTX1 towards SKCa channels, while it was markedly more potent on IKCa1 and several voltage-gated K$^+$ channels.

Key words: chemical synthesis, cobatoxin 1, docking simulation, K$^+$ channel, scorpion toxin, three-dimensional structure.

INTRODUCTION

CoTX1 (cobatoxin 1) is a C-terminal amidated 32-residue toxin with three disulphide bridges that has been isolated from the venom of the Mexican scorpion *Centruroides noxius* Hoffmann [1]. The toxin belongs to a novel family of scorpion toxins, referred to as α-KTx9 [1,2]. So far, only two members of this family have been defined, CoTX1 (α-KTx9.1) and CoTX2 (cobatoxin 2; α-KTx9.2). The primary structures of CoTX1 and CoTX2 present less than 45% sequence identity with other characterized α-KTx members. Since these toxins belong to a new family of scorpion toxins because of their low sequence identities with other K$^+$ channel-acting peptides, combined with the increasing number of discovered K$^+$ channels, a detailed analysis of CoTX1 may provide a valuable opportunity to further characterize the large array of these ion channel types. At a

structural level, CoTX1 possesses the consensus motif of scorpion toxins ...C$_1$...C$_2$XXXC$_3$...(G/A/S)XC$_4$...C$_5$XC$_6$...[3]. It is therefore expected to fold according to the standard α/β scaffold of scorpion toxins with a C$_1$-C$_4$, C$_2$-C$_5$ and C$_3$-C$_6$ disulphide bridge arrangement [1]. At a pharmacological level, CoTX1 reportedly blocks K$_v$ (mammalian voltage-gated)-type K$^+$ channels [*Shaker* B (insect voltage-gated) and K$_v$1.1 K$^+$ channels] in the micromolar concentration range. The full characterization of CoTX1 has been hampered by its limited quantities in the venom. A more complete characterization of CoTX1, as well as a detailed examination of its structural properties, requires the successful chemical production of the toxin and its analogues.

In this article we report the solid-phase synthesis of CoTX1 and the determination of its properties: disulphide bridge organization, 3-D (three-dimensional) structure in solution (solved by ^{1}H-NMR), pharmacology on diverse target channels and computed

simulation of toxin docking on $K_v1.2$ channels. In addition, we designed, chemically synthesized and characterized a CoTX1 analogue, [Pro[7],Gln[9]]-CoTX1, denoted ACoTX1. These two residue substitutions were first selected to restore the RPCQ motif found in Pi1 and to potentially increase peptide binding on apamin-sensitive SKCa channels (small-conductance Ca^{2+}-activated K^+ channels) [4,5]. The RXCQ motif is indeed present in toxins that potently act on SKCa channels, such as Pi1 [6], apamin [7], leiurotoxin 1 [8], PO5 [9] and Tsk [10]. Second, these mutations were also chosen to affect the CoTX1 dipole moment (electric charge anisotropy) in a way by which it is expected to decrease peptide activity on K_v-type K^+ channels [11]. The experimental data show that, contrary to these expectations, the activity of ACoTX1 is similar to that of CoTX1 for SKCa channels, whereas it is more potent on other K^+ channel subtypes [IKCa1 channels (intermediate-conductance Ca^{2+}-activated K^+ channels) and several voltage-gated K^+ channels]. This indicates that the RPCQ motif presents a somehow secondary role regarding peptide binding to SKCa channel, and also suggests that charge anisotropy of CoTX1 does not guide its bioactivity on K^+ channels.

MATERIALS AND METHODS

Materials

Fmoc [N^α-(9-fluorenyl)methyloxycarbonyl]-L-amino acids, Fmoc-amide resin and reagents used for peptide synthesis were obtained from Perkin-Elmer. Solvents were analytical-grade products and purchased from SDS. Enzymes (trypsin and chymotrypsin) were obtained from Roche Molecular Biochemicals.

Chemical synthesis and characterization of CoTX1 and ACoTX1

The CoTX1 and ACoTX1 peptides were obtained by the solid-phase technique [12] using a peptide synthesizer (model 433A; Applied Biosystems). Peptide chains were assembled stepwise on 0.25 mmol of Fmoc-amide resin (0.66 mmol of amino group/g) using 1 mmol of Fmoc-amino acid derivatives. The side-chain-protecting groups used for trifunctional residues were: trityl for Cys, Asn and Gln; t-butyl for Ser, Tyr, Thr and Asp; pentamethylchroman for Arg; and t-butyloxycarbonyl for Lys. The Fmoc-amino acid derivatives were coupled (20 min) as their hydroxybenzotriazole active esters in N-methylpyrrolidone (4-fold excess). The peptide resins (≈ 2 g) were each treated for 3 h at 25 °C with a mixture of TFA (trifluoroacetic acid)/water/thioanisole/ethanedithiol (88:5:5:2, by vol.) in the presence of crystalline phenol (2.2 g). After filtration of the mixtures, the crude peptides were precipitated and washed by adding cold diethyloxide. The crude peptides were pelleted by centrifugation (3000 $\boldsymbol{g}$; 10 min) and the supernatants were discarded. The reduced CoTX1 and ACoTX1 were then dissolved at 2 mM peptide concentrations in 0.2 M Tris/HCl buffer, pH 8.3, and stirred under air to allow oxidative folding (48 h, 25 °C). The crude folded/oxidized peptides were purified by reversed-phase HPLC (Perkin-Elmer; C_{18} Aquapore ODS 20 μm, 250 mm × 10 mm) by means of a 60 min linear gradient of 0–35 % buffer B [0.08 % (v/v) TFA in acetonitrile; where buffer A is 0.1 % (v/v) TFA in water] at a flow rate of 5 ml/min ($\lambda = 230$ nm). The homogeneity and identity of synthetic CoTX1 (CoTX1) or ACoTX1 were assessed by (i) analytical C_{18} reversed-phase HPLC, (ii) amino acid analysis after acidolysis, (iii) Edman sequencing and (iv) mass determination by MALDI-TOF (matrix-assisted laser-desorption ionization–time-of-flight) MS.

Assignment of CoTX1 half-cystine pairings by enzyme-based cleavage of the peptide

CoTX1 (500 μg) was incubated with a mixture of trypsin and chymotrypsin at 10 % (w/w) in 0.2 M Tris/HCl, pH 7.4, for 12 h at 37 °C. The resulting peptide fragments were then purified by reversed-phase HPLC (Vydac C_{18}, 5 μm, 4 mm × 150 mm) with a 60 min linear gradient of 0–60 % buffer B at a flow rate of 1 ml/min ($\lambda = 230$ nm), and freeze dried prior to their analyses. The CoTX1 fragments were hydrolysed by acidolysis (6 M HCl/phenol) and their amino acid contents were determined (Beckman; system 6300 amino acid analyser). The peptide fragments were additionally characterized by MS analysis (RP-DE Voyager; Perseptive Biosystems), and Edman sequencing using a gas-phase microsequencer (Applied Biosystems 470A). Under standard HPLC conditions for analysing phenylthiohydantoin amino acid derivatives, diphenylthiohydantoin-cystine elutes at a retention time of 9.8 min.

CD analysis of the CoTX1 peptides

The CD spectra were recorded on a Jasco J-800 dichrograph. A ratio of 2.20 was found between the positive CD band at 290.5 nm and the negative band at 192.5 nm. CD spectra were reported as the absorption coefficient ($\Delta\varepsilon$) per amide. The far-UV CD spectra were acquired at 20 °C in water between 190 and 260 nm using 0.1 cm-pathlength cell. Data were collected twice at 0.5 nm intervals with a scan rate of 50 nm/min. As assessed by amino acid analyses, the concentrations of CoTX1 or ACoTX1 in the samples were 0.1 mg/ml.

3-D structure determination of CoTX1 in solution by ^{1}H-NMR

NMR spectroscopy

A sample of 0.5 ml of CoTX1 at 5 mM concentration in water/^2H_2O (9:1, v/v) at pH 3.0, uncorrected for isotope effects, was used for recordings of the NMR spectra. Spectral acquisition of all ^{1}H-NMR data was achieved as described previously [13–15]. NOESY spectra were acquired using mixing times of 80 and 120 ms. Clean TOCSY was performed with a spin-lock field strength of 8 kHz and spin-lock time of 80 ms. The amide proton exchange experiments were recorded immediately after dissolution of CoTX1 in ^2H_2O. A series of NOESY spectra with mixing times of 80 ms were recorded at 300 K, the first one for 1 h, followed by spectra of 10 h each. Furthermore, we obtained the NOE (nuclear Overhauser effect) build-up curves by successively recording NOESYs with 50, 150, 200 and 300 ms mixing times in order to check for spin diffusion.

Data processing

Spectra were processed with Bruker's UXNMR software, running on Silicon Graphics Indy R4400 computer. The matrices were transformed to a final size of 2048 points in the acquisition dimension and to 1024 points in the other, except for coupling constant determination for which a 8192 × 1024 matrix was used. The signal was multiplied by a shifted sine bell window in both dimensions prior to a Fourier transformation, then a fifth-order polynomial baseline correction was applied.

Spectral analysis

The identification of amino acid spin systems and the sequential assignment were achieved using the standard strategy described by Wüthrich [16], applied with the graphics software XEASY [17].

Experimental restraints

The integration of NOE data was achieved by measuring the peak volumes. On the basis of known distances in regular secondary structures ($d_{H\alpha\text{-}H\alpha} = 0.23$ nm and $d_{HN\text{-}HN} = 0.33$ nm between two strands of an anti-parallel β-sheet; where HN is amide proton), these volumes were translated into upper limit distances by the CALIBA (calibration of NOE intensity versus distance bonds) routine [18] of DIANA (distance geometry algorithm for NMR) [19] software. All parameters used in the calculations were identical to those used in [20]. The value of the $^3J_{HN\text{-}H\alpha}$ coupling constant was obtained from the first local minimum. The $^3J_{HN\text{-}H\alpha}$ coupling constants were translated into angle restraints using HABAS from the DIANA [19].

Structure calculations

Distance geometry calculations were performed with the variable target function program DIANA 2.8. A preliminary set of 1000 structures was initiated including only intraresidual and sequential upper limit distances. From these, the 500 best were selected for a second round, including medium-range distances, and the resulting 250 best for a third one, with the whole set of upper limit restraints, and some additional distance restraints, used to define the disulphide bridges (i.e. $d_{S\gamma,S\gamma} = 0.21$ nm, $d_{C\beta,S\gamma}$ and $d_{S\gamma,C\beta} = 0.31$ nm). Starting from the 50 best structures, a REDAC (redundant dihedral angle constraints) strategy [19] was used in the last step to include the dihedral restraints together with the additional distance restraints coming out from hydrogen bonds. Final energy refinement was achieved by CNS (crystallography and NMR system; a software suite for macromolecular structure determination) [25]. The visual analysis was carried out with Turbo-Frodo software [21]. The geometric quality of the resulting CoTX1 structures was assessed using PROCHECK 3.3 and PROCHECK-NMR software [22].

Molecular modelling of ACoTX1 and the voltage-gated K$^+$ channels (S5-H5-S6 pore domains)

The molecular modelling of K_v channel subtypes (S5-H5-S6 pore domains) has been achieved on the basis of the crystal structure of part of the KcsA channel solved at 2.0 Å resolution (PDB accession number 1K4C) [23]. The amino acid sequences of domains S5-H5-S6 of the rat voltage-gated K$^+$ channel α-subunits [24] were aligned with region 26–125 of KcsA. The sequence identities between the K_v-type ion channel regions and KcsA are $\approx 31\%$. For the regions comprised between the two transmembrane segments S5 and S6, the sequence identities with KcsA were $\approx 47\%$. Based on the high degree of similarity, models of the S5-H5-S6 regions of mouse $K_v1.1$ (NCBI accession number P16388), rat $K_v1.2$ (NCBI accession number P15386) and mouse $K_v1.3$ (NCBI accession number P16390) channels were generated by using the Turbo-Frodo software [21]. After Clustal alignments (http://www.ebi.ac.uk/clustalw), the amino acid residue mutations were introduced in the KcsA channel, and the structures of the corresponding K_v channels were minimized by using the CNS software [25]. The final molecular models of the S5-H5-S6 regions of the $K_v1.1$, $K_v1.2$ and $K_v1.3$ channels adopt 3-D structures that are similar to that of the KcsA channel. Of note, the ion channel pore region is formed by four S5-H5-S6 domains.

To create a molecular model of ACoTX1, amino acid residue mutations were performed within the amino acid sequence of CoTX1 (PDB accession number 1PJV). The model of ACoTX1

was found to be closely related to the 3-D structure of CoTX1 in solution. The final minimized molecular model of ACoTX1 showed an α/β scaffold, as found in most scorpion toxins [3].

Electrostatic calculations

The electrostatic calculations together with the dipole moments and related analysis were performed by using the GRASP software [26] running on Silicon Graphics Workstations. The potential maps were calculated with a simplified Poisson–Boltzmann solver [27] on the basis of an AMBER-derived parameter file.

Docking of CoTX1 peptides on to K$_v$1.2 channel

The molecular interaction simulations were performed using the BiGGER docking program [28]. The algorithm used by BiGGER performs a complete and systematic search for surface complementarity (both geometry complementarity and amino acid residue pairwise affinities are considered) between two potentially interacting molecules, and enables an implicit treatment of molecular flexibility. In each case, a population of 1000 candidate protein–protein-docked geometries were selected by BiGGER. In a subsequent step, the putative docked structures were ranked using an interaction scoring function, which combines several interaction terms that are thought to be relevant for the stabilization of protein complexes: geometric packing of the surfaces, electrostatic interactions, desolvation energy and pairwise propensities of the amino acid residue side chains to contact across the molecular interface. In the *ab initio* simulations, the entire molecular surface was searched without any additional information regarding the binding sites. Among the 1000 candidate protein–protein-docked geometries selected, the five best scoring CoTX1–K$_v$1.2 or ACoTX1–K$_v$1.2 channel complexes were further treated with the Turbo-Frodo software, also taking into account the deduced functional maps of voltage-gated K$^+$ channel-acting scorpion toxins (for review see [29]). Finally, a rigid-body minimization was used to minimize the selected complexes. The best energy solutions, corresponding to the most favourable CoTX–K$_v$1.2 and ACoTX–K$_v$1.2 channel complexes were retained. The *de visu* analysis was done using Turbo-Frodo software, and the geometric quality of the structures was assessed by PROCHECK 3.3 [22].

Neurotoxicity of CoTX1 peptides *in vivo*

The peptides were tested *in vivo* for toxicity by determining the 50 % lethal dose (LD$_{50}$) after intracerebroventricular injections into 20 g C57/BL6 mice (animal testing agreement number 006573, delivered by the Ministère de l'Agriculture et de la Pêche, France). Groups of six mice per dose were injected with 5 μl of CoTX1 or ACoTX1 peptide solution containing 0.1 % (w/v) BSA and 0.9 % (w/v) NaCl.

Inhibition of ^{125}I-apamin binding on to SKCa channels from rat brain synaptosomes by CoTX1 peptides

Rat brain synaptosomes were prepared as described previously [30]. Aliquots of 50 μl of 0.1 nM ^{125}I-apamin were added to 400 μl of synaptosome suspension (0.4 mg of protein/ml). Samples were incubated for 1 h at 4 °C with 50 μl of one of a series of concentrations of CoTX1 or ACoTX1 [(5×10^{-4})–10^{-14} M] in 500 μl final volume. The incubation buffer was 25 mM Tris/HCl/10 mM KCl, pH 7.2. The samples were

A

```
CoTX1   -------AVC-VYRTCDKDCKRRG-YRSG-KCINNACKCYPY*   (α-KTx9)
ChTX    ---ZFTNVSCTTSKECWSVCQRLHNTSRG-KCMNKKCRCYS     (α-KTx1)   34%
NTX     ---TIINVKCTSPKQCSKPCKELYGSSAGAKCMNGKCKCYNN*   (α-KTx2)   41%
KTX     --GVEINVKCSGSPQCLKPCKDAG-MRFG-KCMNRKCHCTPK    (α-KTx3)   44%
TsTx-α  ---VFINAKCRGSPECLPKCKEAIGKAAG-KCMNGKCKCYP     (α-KTx4)   44%
LTX     -------AFC-NLRMCQLSCR-SLG-LLG-KCIGDKCECVKH*   (α-KTx5)   34%
Pi1     ------LVKCRGTSDCGRPCQQQTGCPNS-KCINRMCKCYGC*   (α-KTx6)   34%
Pi2     ------TISCTNPKQCYPHCKKETGYPNA-KCMNRKCKCRGR    (α-KTx7)   34%
P01     -------VSC---EDCPEHCSTQK--AQA-KCDNDKCVCEPI    (α-KTx8)   28%
```

B

```
CoTX1    AVCVYRTCDKDCKRRGYRSGKCINNACKCYPY*
ACoTX1   AVCVYRPCQKDCKRRGYRSGKCINNACKCYPY*
```

Figure 1 Amino acid sequence of CoTX1 and comparison with those of representative scorpion toxins of each α-KTx structural family

(**A**) The amino acid sequences of CoTX1 [1], charybdotoxin (ChTX [38]), noxiustoxin (NTX [39]), kaliotoxin (KTX [40]), TsTx-α [41], leiurotoxin 1 (LTX [8]), Pi1 [4], Pi2 [42] and P01 [43] were aligned according to the positions of their half-cystine residues, except for Pi1 which belongs to the particular α-KTx6 family of four-disulphide-bridged scorpion toxins acting on K$^+$ channels. The nine scorpion toxin structural families are noted; α-KTx1–9 [1,2]. Gaps (—) were introduced into the toxin amino acid sequences to maximize homology. The positions of half-cystine residues are highlighted in grey boxes. The asterisk indicates a C-terminal carboxylamidated extremity. Amino acid sequence identities (%) with CoTX1 are shown on the right. (**B**) Amino acid sequences of CoTX1 and its analogue, ACoTX1. The grey box illustrates the four-residue motif that is thought to be important for SKCa channel recognition.

centrifuged and the resulting pellets were washed three times in 1 ml of the same buffer. Bound radioactivity was determined by gamma counting (Packard Crystal II). The values expressed are the means ± S.D. from triplicate experiments. Non-specific binding, less than 10 % of the total binding, was determined in the presence of an excess (10 nM) of unlabelled apamin.

K$^+$ current blockage efficacy of CoTX1 peptides (electrophysiology)

Cells

Stably transfected mammalian cell lines expressing either mouse $K_v 1.1$ (m$K_v 1.1$), rat $K_v 1.2$ (r$K_v 1.2$), mouse $K_v 1.3$ (m$K_v 1.3$), human $K_v 1.5$ (h$K_v 1.5$) or mouse $K_v 3.1$ (m$K_v 3.1$) channels were used [31]. The cell lines were maintained in Dulbecco's modified Eagle's medium containing 4 mM L-glutamine, 1 mM sodium pyruvate (Gibco, Paisley, Scotland, U.K.), 10 % (v/v) heat-inactivated fetal calf serum (PAA Laboratories, Linz, Austria) and 100 μg/ml G418 (Gibco; for cell lines expressing m$K_v 1.1$, r$K_v 1.3$, and m$K_v 3.1$). The tsA cell line expressing hIKCa1 (human IKCa1) channel was a kind gift from Dr D.C. Devor (University of Pittsburg, Pittsburg, PA, U.S.A.). The *Shaker* B Δ44 channel expression construct [a construct expressing a *Shaker* B channel formed by α subunits truncated at their N-terminal extremity (region 1–44); a kind gift from Dr S.H. Heinemann, University of Jena, Jena, Germany] was linearized and transcribed *in vitro*. The cRNA, together with a fluorescent FITC dye, was injected into rat basophilic leukaemia cells. Fluorescent cells were visualized after 4–6 h of incubation, and *Shaker* B Δ44 K$^+$ currents were measured.

Electrophysiological recordings

All the experiments were carried out at room temperature (22–25 °C) using the whole-cell recording mode of the patch–clamp technique [32,33]. Cells were bathed with mammalian Ringer's solution containing 160 mM NaCl, 4.5 mM KCl, 2 mM CaCl$_2$, 1 mM MgCl$_2$ and 10 mM Hepes, pH 7.4 (with NaOH), with an osmolarity of 290–320 mOsm. When CoTX1 peptides were applied, 0.1 % BSA was added to the Ringer's solution. A

simple syringe-driven perfusion system was used to exchange the bath solution in the recording chamber. Electrodes were pulled from glass capillaries (Science Products, Hofheim, Germany) in three stages, and fire-polished to resistances measured in the bath of 2.5–5 MΩ. The internal pipette solution used for measuring voltage-gated K$^+$ currents contained 155 mM KF, 2 mM MgCl$_2$, 10 mM Hepes and 10 mM EGTA, pH 7.2 (with KOH), with an osmolarity of 290–320 mOsm. For measuring K$^+$ currents through IKCa1 channels, an internal pipette solution containing 135 mM potassium aspartate, 8.7 mM CaCl$_2$, 2 mM MgCl$_2$, 10 mM EGTA and 10 mM Hepes, pH 7.2 (with KOH), with an osmolarity of 290–320 mOsm (free $[Ca^{2+}]_i = 10^{-6}$ M), was used. Membrane currents were measured with an EPC-9 patch-clamp amplifier (HEKA Elektronik, Lambrecht, Germany) interfaced to a Macintosh computer running acquisition and analysis software (Pulse and PulseFit). Capacitive and leak currents were subtracted using the P/10 procedure of this software. Series resistance compensation (> 80 %) was employed if the current exceeded 2 nA. The holding potential in all experiments was −80 mV. Data analysis was performed in IgorPro, and K_d values were deduced by fitting a modified Hill equation $\{I_{toxin}/I_{control} = 1/[1 + ([toxin]/K_d)]\}$, with a Hill coefficient of 1, to normalized data points obtained at more than four different CoTX1 peptide concentrations. The value for each peptide concentration was the mean from at least three measurements.

RESULTS AND DISCUSSION

CoTX1, a member of a new family of scorpion toxins

CoTX1 belongs to a new family of α-KTx scorpion toxins (α-KTx9) [1,2]. As shown in Figure 1(A), CoTX1 shares at most 44 % amino acid sequence identity with representative toxins of each α-KTx family. Except toxins of the four-disulphide-bridged α-KTx6 family, CoTX1 is cross-linked by three disulphide bridges similarly to other α-KTx members. CoTX1 displays the consensus sequence . . . C$_1$ . . . C$_2$XXXC$_3$ . . . (G/A/S)XC$_4$ . . . C$_5$XC$_6$ . . . of scorpion toxins [3]. It is therefore expected to fold according to the common α/β scaffold with the disulphide bridge framework of the C$_1$-C$_4$, C$_2$-C$_5$ and C$_3$-C$_6$

A
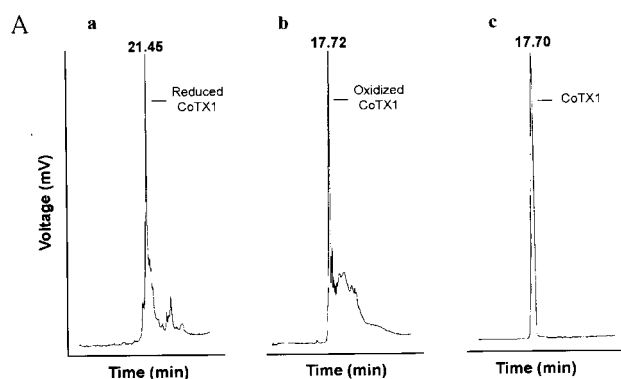
B

Enzymes	Retention time (min)	Proteolytic fragments	Experimental Mr (M+H)⁺	Deduced Mr (M+H)⁺	Half-cystine pairings
Trypsin + Chymotrypsin	22.87	DCK CYPY-NH2 (12, 29)	909.2	908.9	Cys12-Cys29
	23.07	TCDK NACK (8, 27)	901.0	900.9	Cys8-Cys27
	26.83	AVCVY CIN (3, 22)	903.1	903.9	Cys3-Cys22

CoTX1   AVCVYRTCDKDCKRRGYRSGKCINNACKCYPY-NH2

Figure 2   CoTX1 at various stages of chemical synthesis and characterization thereof

(**A**) Analytical C_{18} reversed-phase HPLC profiles of CoTX1 (**a–c**) at different stages of its chemical synthesis. (**a**) the crude reduced peptide after final TFA treatment. (**b**) The crude peptide after 48 h of oxidative folding. (**c**) The purified folded/oxidized CoTX1. (**B**) Assignment of CoTX1 half-cystine pairings by enzyme-based cleavage of the synthetic toxin. The CoTX1 fragments were generated by trypsin/chymotrypsin cleavage and characterized (see in Materials and methods section). Retention times in HPLC and identified half-cystine pairings of the peptides are shown. The disulphide bridge organization of CoTX1, as experimentally established by partial proteolysis of the synthetic toxin, is shown below. The half-cystine residues are numbered according to their positions in the CoTX1 amino acid sequence. The disulphide bridges are represented by solid lines.

type. Such a scaffold consists of a helical structure connected to an anti-parallel β-sheet by two disulphide bridges. CoTX1 has a shorter N-terminal domain than toxin members of the α-KTx1–4 families indicating that it possesses a two- rather than a three-stranded β-sheet. The primary structures of both CoTX1 and its analogue ACoTX1 are presented in Figure 1(B). The two residue substitutions made in CoTX1 amino acid sequence are located in a domain that presumably forms a helical structure [1].

Chemical syntheses and characterizations of CoTX1 and its analogue ACoTX1

Solid-phase chemical syntheses of CoTX1 and ACoTX1 were achieved stepwise on 0.25 mmol of Fmoc-amide resin by means of an Fmoc/t-butyl strategy [12]. In both cases, the amount of target peptide linked to the resin was ≈ 0.2 mmol, indicating an 80 % yield of peptide assemblies. Accordingly, a relative homogeneity of each crude reduced peptide was obtained after TFA treatment, as assessed by analytical C_{18} reversed-phase HPLC (see Fig-
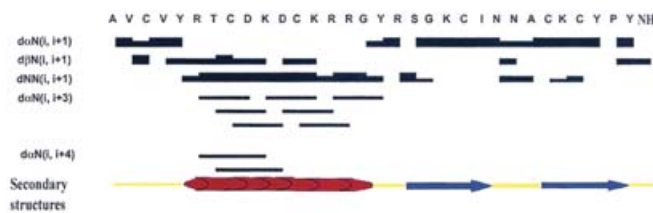

Figure 3   Analyses of CoTX1 secondary structures

Surveys of the ¹H-NMR sequential assignments of CoTX1. The intensities of sequential NOE, extracted from NOESY with mixing times of 80 ms, are represented by the thickness of bars. The secondary structures of CoTX1, α-helix (red) and β-sheet (blue), are summarized at the bottom.

Table 1   Chemical shifts of CoTX 1 at 300 K

Residue	HN	HCα	HCβ	Other
A¹	7.74	4.08	1.46	
V²	8.37	4.25	1.95	HCγ¹, 0.86; HCγ², 0.86
C³	8.30	4.40	2.76, 2.47	
V⁴	8.73	4.22	1.99	HCγ¹, 1.02; HCγ², 0.91
Y⁵	9.07	4.03	3.34, 2.92	HCγ, 6.95; HCγ, 7.09
R⁶	8.70	3.55	1.78, 1.66	HCγ, 1.53, 1.53; HCδ, 3.15, 3.15; HNε, 5.67
T⁷	6.72	3.92	3.97	HCγ², 1.15
C⁸	8.31	4.46	3.19, 2.45	
D⁹	8.61	3.88	2.49, 2.26	
K¹⁰	7.48	3.71	1.79, 1.54	HCγ, 2.90; HNζ, 7.53
D¹¹	8.54	4.34	2.95, 2.76	
C¹²	8.60	4.27	2.60, 2.48	
K¹³	8.17	4.55	1.86, 1.74	HCγ, 3.01; HCδ, 1.55, 1.33; HNζ, 7.64
R¹⁴	8.28	4.10	2.02, 2.02	HCγ, 3.24, 3.16; HCδ, 1.75; HNε, 7.18
R¹⁵	7.46	4.35	1.98, 1.89	HCγ, 3.20, 2.40; HCδ, 1.74; HNε, 6.67, 7.13
G¹⁶	7.71	3.76, 4.15		
Y¹⁷	7.91	4.53	3.20, 2.34	HCγ 6.67, 6.90
R¹⁸	8.33	3.60	1.27, 1.27	HCγ, 2.99; HCδ, 0.57; HNε, 5.65
S¹⁹	7.67	4.27	4.16, 3.88	
G²⁰	8.73	4.13, 5.49		
K²¹	8.94	4.53	1.84, 1.84	HCγ, 1.54, 1.47, 1.33; HCδ, 2.77; HNε, 7.32
C²²	8.34	5.14	2.79, 2.80	
I²³	9.06	3.88	1.73	HCγ¹, 1.14, 1.32; HCγ², 0.82
N²⁴	9.52	4.26	2.99, 2.71	
N²⁵	8.90	4.18	3.12, 2.74	HNδ2, 6.85, 7.55
A²⁶	7.95	4.54	1.28	
C²⁷	8.65	4.65	2.96, 2.55	
K²⁸	9.22	4.40	1.70, 1.62	HCγ, 1.48, 1.00; HCδ, 2.76, 2.70; HNζ, 7.40
C²⁹	8.05	5.30	2.03, 1.16	
Y³⁰	8.49	4.46	2.85, 2.67	Cγ, 6.60, 7.19
P³¹	–	4.86	2.35, 2.28	HCγ, 2.17, 2.00; HCδ, 4.10, 4.06
Y³²	8.46	4.19	3.09, 2.84	

ure 2A, which illustrates the case of CoTX1). Finally, the crude peptides were folded/oxidized for 48 h under alkaline conditions, and the main oxidized species (CoTX1 and ACoTX1) were purified to >99 % homogeneity by preparative C_{18} reversed-phase HPLC. Amino acid analyses of the purified products show amino acid ratios that are consistent with the values deduced from their primary structures (results not shown). The MS analyses (MALDI-TOF technique) of the peptides gave experimental molecular masses $(M + H)^+$ of 3731.8 and 3752.4, which are similar to the deduced molecular masses $(M + H)^+$ of 3731.4 and 3752.2 calculated for CoTX1 and ACoTX1, respectively. The yield of each chemical synthesis, which combines yields of peptide assembly, final TFA treatment, oxidative folding and purification, was ≈ 4 %.
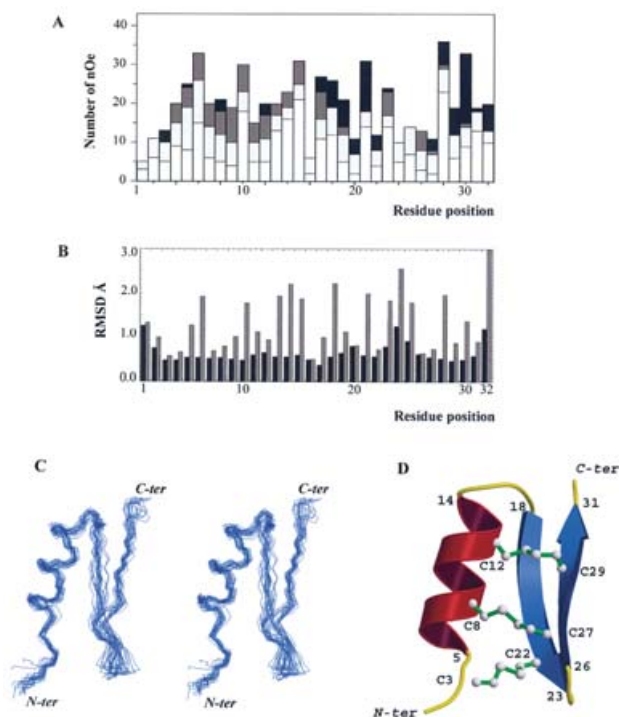
Figure 4   3-D structure of CoTX1 in solution, as determined by ^{1}H-NMR

(**A**) Distribution of NOE constraints per residue along the amino acid sequence of CoTX1. The NOE constraints are separated into intra-residue (white), sequential (light grey), medium-range (dark grey) and long-range (black). (**B**) Local values of averaged r.m.s.d. (Å) calculated from the 20 best CoTX1 solution structures. The CoTX1 backbone and residue side chains are shown in black and grey, respectively. (**C**) Stereo views of the 20 best molecular CoTX1 structures (only backbone atoms are displayed) superimposed for best fit. N-ter and C-ter correspond to N- and C-terminal extremities. (**D**) Molscript ribbon drawing of the averaged minimized CoTX1 structure. The α-helix, anti-parallel β-sheet, Cα backbone trace and disulphide bridges are shown in red, blue, yellow and green, respectively. The six half-cystine residues are numbered according to their positions in the CoTX1 amino acid sequence. Other residues noted are those that start or end a secondary structure.

Table 2   Structural statistics of the 20 best structures

The r.m.s.d. values are calculated with respect to the mean structure. (DG) are the final 20 CoTX 1 structures obtained by distance geometry and energy minimization. $\langle \overline{DG} \rangle$ is the mean structure obtained by averaging the co-ordinates of the individual DG structures best fitted to each other. The square-well NOE (E_{NOE}) was calculated with a force constant of 75 kcal $\cdot$ mol^{-1}. The square-well torsional angle E_{tor} was calculated with a force constant of 200 kcal $\cdot$ mol^{-1}. The quadratic van der Waals term was calculated with a force constant of 4 kcal $\cdot$ mol^{-1} and the van der Waals radii were set to 0.78 times the standard CHARMm values. The r.m.s.d. values were obtained by best fitting the backbone atom co-ordinates for residues 1–32 of the 20 individual structures. The given numbers for the backbone and all heavy atoms represent the means $\pm$ S.D. of pairwise values.

	(DG)	$\langle \overline{DG} \rangle$
Backbone (C, Cα, N) r.m.s.d. (Å)	0.52 ± 0.13	
All heavy atoms r.m.s.d. (Å)	1.14 ± 0.15	
Energies (kcal/mol)		
Total	29.26 ± 5.96	31.10 ± 4.81
Bonds	1.213 ± 0.42	1.27 ± 0.26
Angles	17.46 ± 3.06	17.59 ± 1.64
Improper	0.73 ± 0.28	0.77 ± 0.18
Van der Waals (repel)	5.88 ± 3.52	6.53 ± 2.16
NOE	4.94 ± 0.51	4.94 ± 1.33
r.m.s.d. from ideal value		
Bonds (Å)	$1.57 \times 10^{-3} \pm 2.0 \times 10^{-4}$	$1.6 \times 10^{-3} \pm 1.6 \times 10^{-4}$
Angles (°)	0.317 ± 0.02	0.35 ± 0.016
Improper (°)	0.122 ± 0.02	0.13 ± 0.015
Dihedral (°)	30.48 ± 2.3	30.63 ± 1.30
r.m.s.d. from restraints		
NOE (Å)	0.014 ± 0.0025	0.014 ± 0.0019

	Maximum of violation	(DG)	$\langle \overline{DG} \rangle$
Violation from ideal value			
Bonds > 0.05	0	0	0
Angles > 5°	0	0	0
Improper > 5°	0	0	0
Van der Waals < 1.6	0	0	0
Dihedral > 30	29	24.73 ± 2	25
Violation from restraints			
NOE > 0.2 Å	0.29	0.05	0

Disulphide bridge pattern of CoTX1

To assign CoTX1 half-cystine pairings, the peptide was treated by a mixture of trypsin and chymotrypsin, and the resulting fragments were purified by HPLC and characterized by amino acid content determination, Edman sequencing and MS analysis (Figure 2B). The half-cystine pairings were thereby mapped as Cys^3-Cys^{22}, Cys^8-Cys^{27} and Cys^{12}-Cys^{29}. The disulphide bridge organization of CoTX1 is therefore of the C_1-C_4, C_2-C_5 and C_3-C_6 type, a pattern commonly found in three-disulphide-bridged scorpion toxins [29].

CD analysis

The CD spectra of CoTX1 and ACoTX1 were recorded to assess their secondary structures (results not shown). Measurements were performed at a wavelength ranging from 185 to 260 nm. The data obtained correspond essentially to $\pi-\pi^*$ and $n-\pi^*$ transitions of the amide chromophores of the peptide backbones [34]. The CD spectra show large negative contributions between 207 and 230 nm, and large positive contributions between 190 and 200 nm, indicating the presence of both α-helical and β-sheet structures. These data are coherent with peptide backbone folding according to an α/β scaffold [3] for both CoTX1 and ACoTX1.

Determination of the 3-D solution structure of CoTX1

Figure 3 illustrates the determination of the 3-D solution structure of CoTX1. The qualitative analysis of sequential NOE intensities for secondary structure determination, together with the pattern of medium-range constraints, allowed us to predict a helical conformation between Tyr^5 and Gly^{15} for CoTX1. There are some strong sequential HN(i) − HN(i + 1), weak or no Hα(i) − HN(i + 1), and a stretch of medium-range NOE in this region for CoTX1. On the basis of the qualitative analyses of CoTX1, we detected two extended fragments, one from Arg^{18} to Ile^{23} and another from Ala^{26} to Pro^{31} [strong Hα(i) − HN(i + 1) together with weak HN(i) − HN(i + 1) sequential NOE]. These two strands are connected by a tight turn centred on Asn^{24} and Asn^{25}. The N-terminal fragment is an extended conformation from Ala^1 to Val^2. For structure calculations, sequential assignments of CoTX1 were achieved first by the standard method of Wüthrich [16], and second, most protons were identified and the resonance frequencies determined (Table 1). The structures of CoTX1 were determined by using 348 NOE-based distance restraints (135 intra-residue, 82 sequential, 52 medium-range and 79 long-range restraints). In addition, 28 hydrogen-bond
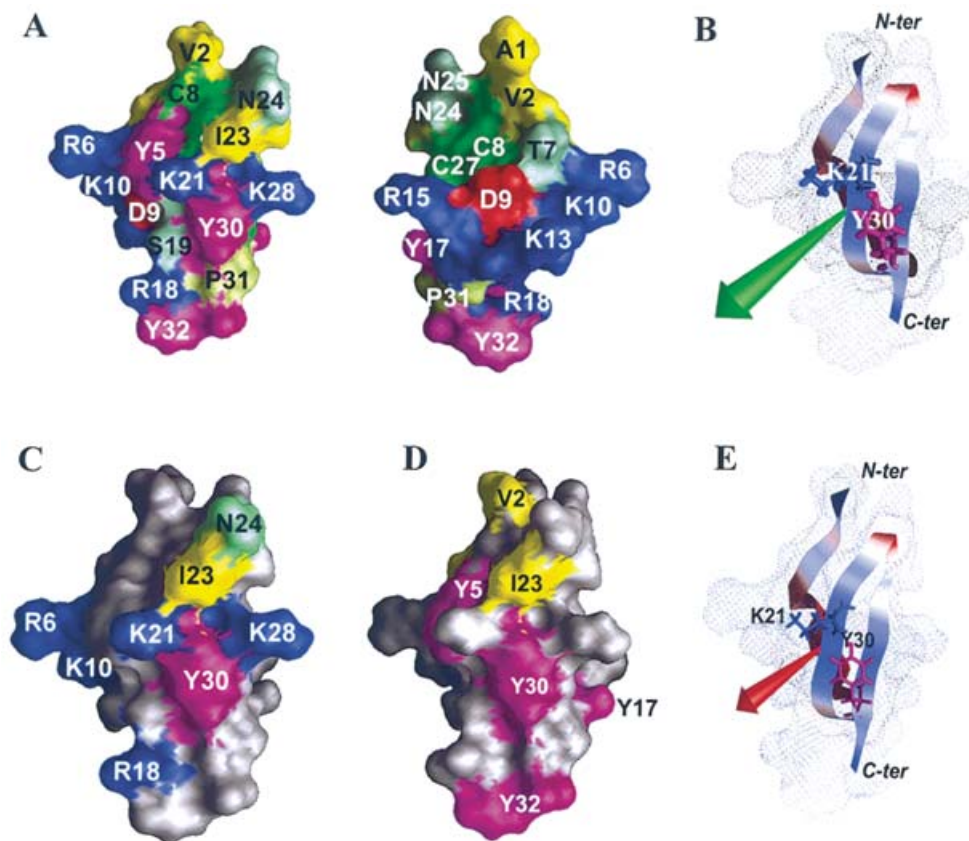
Figure 5   Analyses of CoTX1 and ACoTX1 surfaces

(**A**) Representations of the CoTX1 molecular surface. The amino acid residues from either the β-sheet (left-hand panel) or the α-helix (right-hand panel) are indicated. Colour codes: yellow (hydrophobic residues), light green (polar residues), dark green (half-cystine residues), red (acidic residues), blue (basic residues) and pink (aromatic residues). Note that the CoTX1 surface is mainly covered by hydrophilic residues. (**B**) Electrostatic surface analysis of CoTX1. Ribbon (worm) representation of Cα-trace. Red and blue denote negative and positive electric charges, respectively. Colour variations correspond to differences in electric charge intensities. For residues belonging to the functional dyad (K^{21} and Y^{30}), the side-chains are detailed in balls and sticks. The anisotropy of electric charge distribution (dipole moment) is represented by the green arrow. The size of the arrow is proportional to the intensity of anisotropy. (**C**–**E**) Modelled structure of ACoTX1. Functional map (**C**, β-sheet side), hydrophobic surface (**D**, β-sheet side) and ribbon representation (**E**) of ACoTX1. Note that the dipole moment (red) of ACoTX1 is reduced by 2-fold compared with that of CoTX1.

restraints (derived from hydrogen-exchange data) have been included, as well as nine distance restraints derived from the three disulphide bridges. Altogether, the final experimental set corresponds to 12 constraints per residue on average (Figure 4A). The structures were calculated by using a hybrid distance geometry-simulated annealing protocol using distance geometry algorithm for NMR (DIANA [19]) and CNS [25]. The best-fit superimposition of backbone atoms for 20 models gives r.m.s.d. (root mean square deviation) values of 0.52 Å for backbone atoms and 1.14 Å if all known hydrogen atoms are included (Figure 4B; Table 2). The local r.m.s.d. values are represented on Figure 4(B) and show that the precision of the calculation is quite constant all along the CoTX1 amino acid sequence. A summary of the structural statistics is given in Table 2. All the 20 CoTX1 solution structures (Figure 4C) have good non-bonded contacts and covalent geometry, as evidenced by low values of CNS energy terms. The correlation with the experimental data shows no NOE-derived distance violation greater than 0.2 Å. Also, the analysis of the Ramachandran plot shows (according to PROCHECK standard nomenclature) 83 % of the residues in the most favoured regions, 17 % in the additional favoured regions and none in the generously allowed or disallowed regions. The 3-D structures (PDB accession code 1PJV) of CoTX1 consist of

an homogeneous family, sharing the same fold: a two-stranded β-sheet and an α-helix (Figure 4D). The precise localization of these secondary structures has been defined by PROCHECK-NMR, which indicates the presence of a α-helix running from Tyr[5] to Arg[14] (two turns of helix), and a double-stranded anti-parallel β-sheet made of the Arg[18]–Ile[23] and Ala[26]–Tyr[30] portions. This β-sheet is right-hand twisted and stabilized by six hydrogen bonds. The α-helix is connected to the β-sheet by a tight turn formed by the region Arg[15]–Tyr[17]. The two strands of the β-sheet are connected by a well-defined type I′ β-turn formed by the Asn[24] and Asn[25] residues (Figure 4D). Of note, the angle between the axis of the α-helix and that of the β-sheet is close to 0°. These secondary structures fully agree with the experimental data presented in Figure 3(B) and Figure 4(A). The current 3-D solution structure determination of CoTX1 concerns the synthetic molecule. It most probably also reflects the 3-D structure of the native CoTX1 that could not be determined due to its current unavailability. However, several points argue in favour of their full identity. First, the 3-D solution structure of synthetic CoTX1 is remarkably similar to the molecular model previously generated by Selisko and co-workers [1]. Second, the oxidative folding process *in vitro* of reduced synthetic CoTX1 resembles those of other K^{+} channel-acting toxins of known 3-D structures [6,9,10].
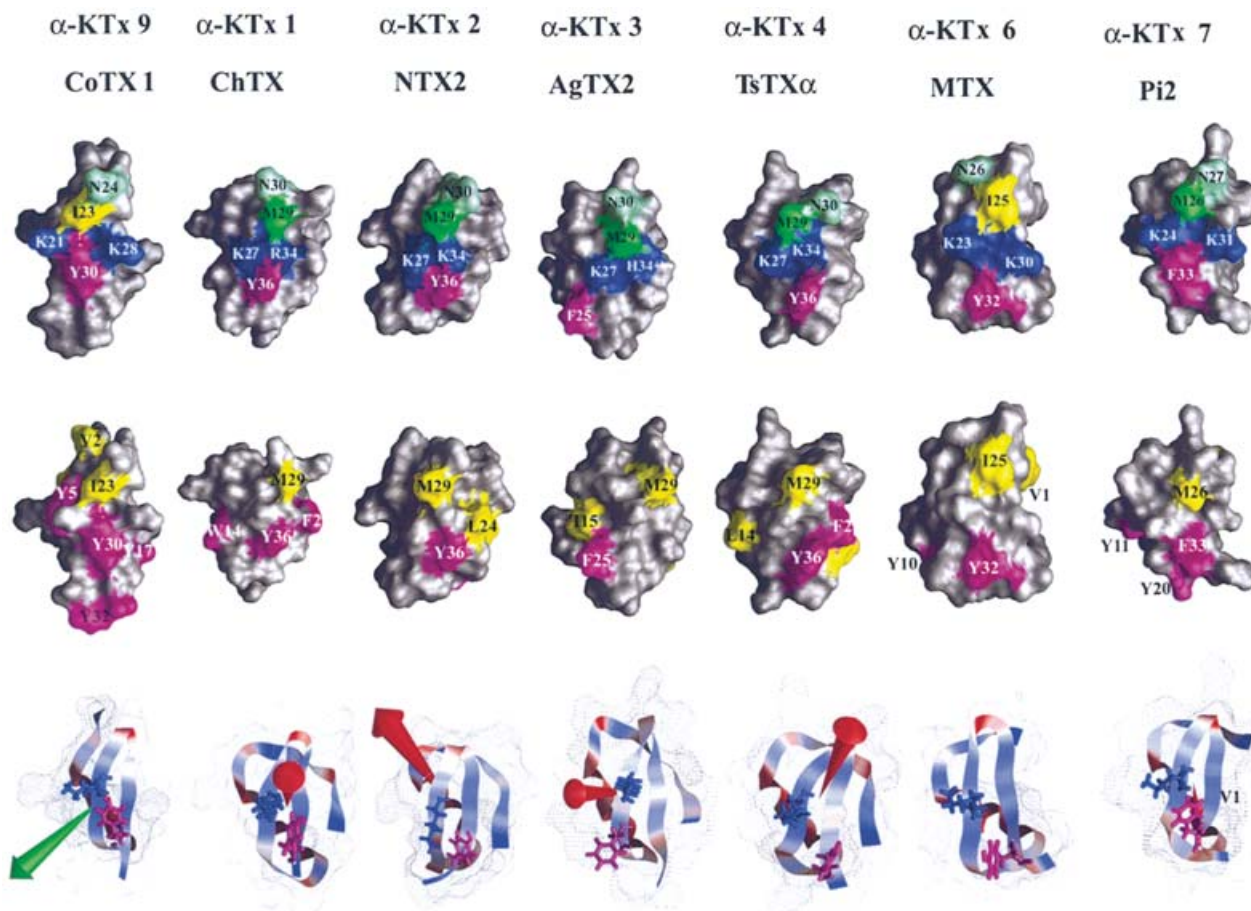
Figure 6   Comparison of CoTX1 interacting surface with those of other representative members of the α-KTx family

Functional maps depicting amino acid residues that are key for toxin interaction with K_v-type channels (top row, β-sheet side), hydrophobic surfaces (middle row, β-sheet side) and ribbon representations (bottom row) of CoTX1 and other K_v channel-acting toxins representative (9, 1–4, 6 and 7) of the α-KTx family. The dipole moments of representative toxins (red) are compared with that of CoTX1 (green). Colour codes used for the amino acid residues are as in Figure 5(A). Note that amino acid residues belonging to the basic ring of CoTX1 are omitted for the sake of comparison with other toxins. MTX, maurotoxin (a scorpion toxin from *Scorpio maurus palmatus* venom); AgTX2, agitoxin 2 (a scorpion toxin from *Leiurus quinquestriatus hebraeus*); other toxin names are defined in Figure 1.

Third, the half-cystine pairing pattern experimentally determined for folded/oxidized synthetic CoTX1 is identical to those of other three-disulphide-bridged scorpion toxins acting on K^+ channels (i.e. C_1-C_4, C_2-C_5 and C_3-C_6), strongly suggesting the occurrence of a correct folding *in vitro*. Finally, we also evidenced an α/β-scaffold for synthetic CoTX1, consistent with all known 3-D solution structures of related toxins.

Surface analysis of CoTX1

The surface of CoTX1 is predominantly composed of polar and hydrophilic amino acid residues. Indeed, all four Lys, four Arg, two Asn and two Asp residues are exposed to the solvent (Figure 5A). All the polar residues are in contact with the solvent, although no well-defined salt bridges can be detected at the CoTX1 surface. In the complete bundle of NMR solutions, most of the exposed residue-side-chains are mobile (Figures 4B and 4C). A number of hydrophobic residues (Ala[1], Val[2], Val[4] and Ile[23]) form a solvent-exposed hydrophobic cluster on one side of the molecule. Another hydrophobic cluster, located at the opposite side of CoTX1, is composed of Tyr[17], Tyr[30] and Tyr[32], packed against Pro[31].

The dipole moment of CoTX1 resulting from its charge-distribution anisotropy is shown by an arrow on Figure 5(B). It is directed from the centre of the molecule and oriented from the lowest to the highest positive charge density. The size of the arrow is proportional to the intensity of the anisotropy. It emerges from the molecule through a basic-rich surface (Arg[6], Lys[10], Lys[13], Arg[14] and Lys[21]; only one acidic Asp[8] residue); the opposite face being poorly basic (Arg[15] and Lys[28]; and one acidic Asp[9] residue).

Structural comparison between CoTX1 and toxins from other α-KTx families

The comparison of the 3-D structure of CoTX1 with those of other structurally well-characterized toxins from the diverse families highlights the conservation of five specific amino acid residues (Lys[21], Ile[23], Asn[24], Lys[28] and Tyr[30]) reportedly critical for voltage-gated K^+ channel blockage (Figure 6, top row; for a review see [29]). This observation is in line with the ability of CoTX1 to block *Shaker* B and $K_v1.1$ channels [1]. One striking difference carried by CoTX1 over other toxins is the presence of two hydrophobic residue clusters located at either side of its functional dyad (Lys[21] and Tyr[30]; Figure 6, middle row). This

property, combined with a longer α-helix, makes CoTX1 less globular than other characterized toxins. It is noteworthy that some hydrophobic clusters can also be found in other toxins, although they are generally not distributed in such a diametrically opposite manner. An analysis of the dipole moment of CoTX1 reveals that it exhibits a charge anisotropy similar to those of toxins active on both K_v and SKCa K^+ channels (Figure 6, bottom row).

Apart from the toxin functional maps, it has also been proposed that the peptide dipole moments could be pivotal for K^+ channel recognition and blockage [11]. To investigate this point, we designed and chemically synthesized a structural analogue of CoTX1, termed ACoTX1, with the aim of decreasing the intensity but not the orientation of the dipole moment. ACoTX1 presents two amino acid residue substitutions as compared with CoTX1, i.e. Pro^7 and Gln^9 instead of Thr^7 and Asp^9. The residue mutation from Asp^9 to Gln^9 affects the intensity of the dipole moment by altering an amino acid residue that is located at the centre of the face opposite to the β-sheet interacting surface. In addition, Thr^7 was replaced by Pro^7 to eliminate the potential contribution of the hydroxyl side-chain of Thr to the dipole moment. A Pro residue was selected because (i) of its neutral nature regarding the dipole moment and (ii) it restores the RPCQ motif found in Pi1, a toxin that potently acts on SKCa channels [6].

Modelled structure of ACoTX1

To generate a molecular model of ACoTX1, residue replacements were performed within the 3-D structure of CoTX1 using the Turbo-Frodo software [21]. The structure of ACoTX1 was refined by molecular annealing dynamics, followed by energy minimization using the CNS software. Figure 5(C) illustrates that the refined molecular model of ACoTX1 has a similar distribution of toxin key residues for K_v channel blockage. Also, the distribution of the two clusters of hydrophobic residues are maintained within ACoTX1 (Figure 5D). However, the molecular dipole moment presents the same orientation as that of CoTX1, but is markedly decreased in intensity (Figure 5E). This situation appears to be convenient to address the relative importance of the dipole moment in toxin bioactivity.

Bioactivities of CoTX1 and ACoTX1

CoTX1 and ACoTX1 were tested *in vivo* for neurotoxicity by intracerebroventricular injections in C57/BL6 mice. Both peptides are lethal in mice, with LD_{50} values of 500 ± 45 ng/mouse (CoTX1, $n = 48$ mice) and 300 ± 32 ng/mouse (ACoTX1, $n = 48$ mice). This lethal activity is 10–20-fold less potent than other known three-disulphide-bridged scorpion toxins [9,10]. Of note, ACoTX1 displays an increased lethal activity compared with its natural counterpart.

To investigate the pharmacological actions of CoTX1 and ACoTX1, we first tested their abilities to compete with ^{125}I-apamin for binding on to SKCa channels of rat brain synaptosomes (Figure 7A). Both peptides inhibit ^{125}I-apamin binding with IC_{50} values of 7.2 ± 0.2 μM (CoTX1) and 4.8 ± 0.2 μM (ACoTX1). The affinity of these two peptides for SKCa channels thus appears weak. Next, we evaluated the effects of CoTX1 and ACoTX1 on hIKCa1 expressed in the tsA cell line [35,36] (Figure 7B). Both peptides fully inhibit hIKCa1 K^+ currents with IC_{50} values of 484 ± 62 nM (CoTX1) and 73 ± 7 nM (ACoTX1). ACoTX1 is thus 6.5-fold more active than CoTX1 for interacting with hIKCa1. These data are the first evaluating CoTX1 activity towards Ca^{2+}-activated K^+ channels.
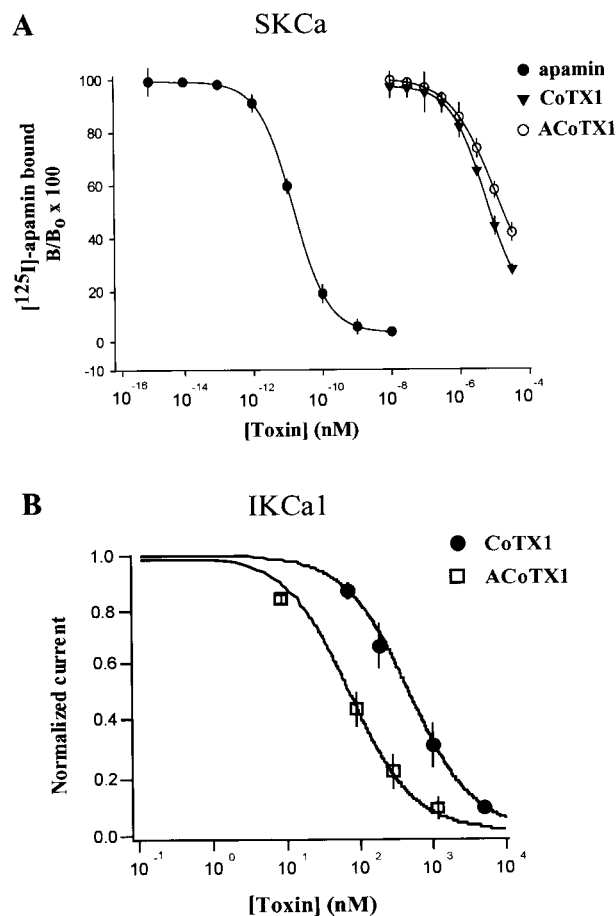
Figure 7   Activities of CoTX1 and ACoTX1 towards Ca^{2+}-activated K^+ channels

(**A**) Concentration-dependent inhibition of binding of ^{125}I-apamin to rat brain synaptosomes by unlabelled apamin (●), CoTX1 (▼) or ACoTX1 (○) in a competition assay. B_0 is the binding of ^{125}I-apamin without addition of any other ligand, and B is the binding in the presence of the indicated concentrations of competitor. Non-specific binding, less than 8 % total binding, was subtracted for the calculation of ratios. When absent, error bars are within symbol size. The data were fitted by the equation $y = y_0 + a/[1 + \exp(-(x - IC_{50})/b)]$. The IC_{50} values were 7.2 ± 0.2 μM (CoTX1), 4.8 ± 0.2 μM (ACoTX1) and 15.6 ± 3 pM (unlabelled apamin). Binding experiments have been performed in triplicate. (**B**) Concentration–response curve for inhibition of IKCa1 currents by increasing concentrations of either CoTX1 (●) or ACoTX1 (□). Data points are means $\pm$ S.D. from at least three experiments. The data were fitted by a modified Hill equation ($I_{peptide}/I_{control} = 1/[1 + ([peptide]/K_d)]$) with a Hill coefficient of 1, revealing a K_d of 484 ± 62 nM for CoTX1 and 73 ± 7 nM for ACoTX1.

We also tested the effects of both peptides on voltage-gated K^+ channels expressed in mammalian cell lines (Figure 8). Dose–response curves were obtained for rat $K_v 1.2$, mouse $K_v 1.3$ and $K_v 1.1$, and *Shaker* B $\Delta 44$ K^+ channels. The K_d values obtained for CoTX1 were 27 ± 4 nM ($K_v 1.2$), 5.3 ± 1.3 μM ($K_v 1.3$), 24.4 ± 4 μM ($K_v 1.1$) and 1.0 ± 0.1 μM (*Shaker* B $\Delta 44$). The K_d value obtained for synthetic CoTX1 effect on *Shaker* B $\Delta 44$ is close to the value reported for native CoTX1 effect on *Shaker* B (reported K_d value of 0.7 μM [1]). In contrast, we report a lower affinity (≈ 49-fold) for mouse Kv1.1 channels than the one reported by Selisko and collaborators [1]. This difference may be attributed to the distinct cell expression system used (mammalian cell line versus *Xenopus* oocytes). In comparison, ACoTX1 is significantly more active than CoTX1 (up to 20-fold) on these channels, with K_d values of 1.9 ± 0.2 nM ($K_v 1.2$), 260 ± 10 nM ($K_v 1.3$), 7.4 ± 0.9 μM ($K_v 1.1$) and 88 ± 23 nM (*Shaker* B $\Delta 44$).
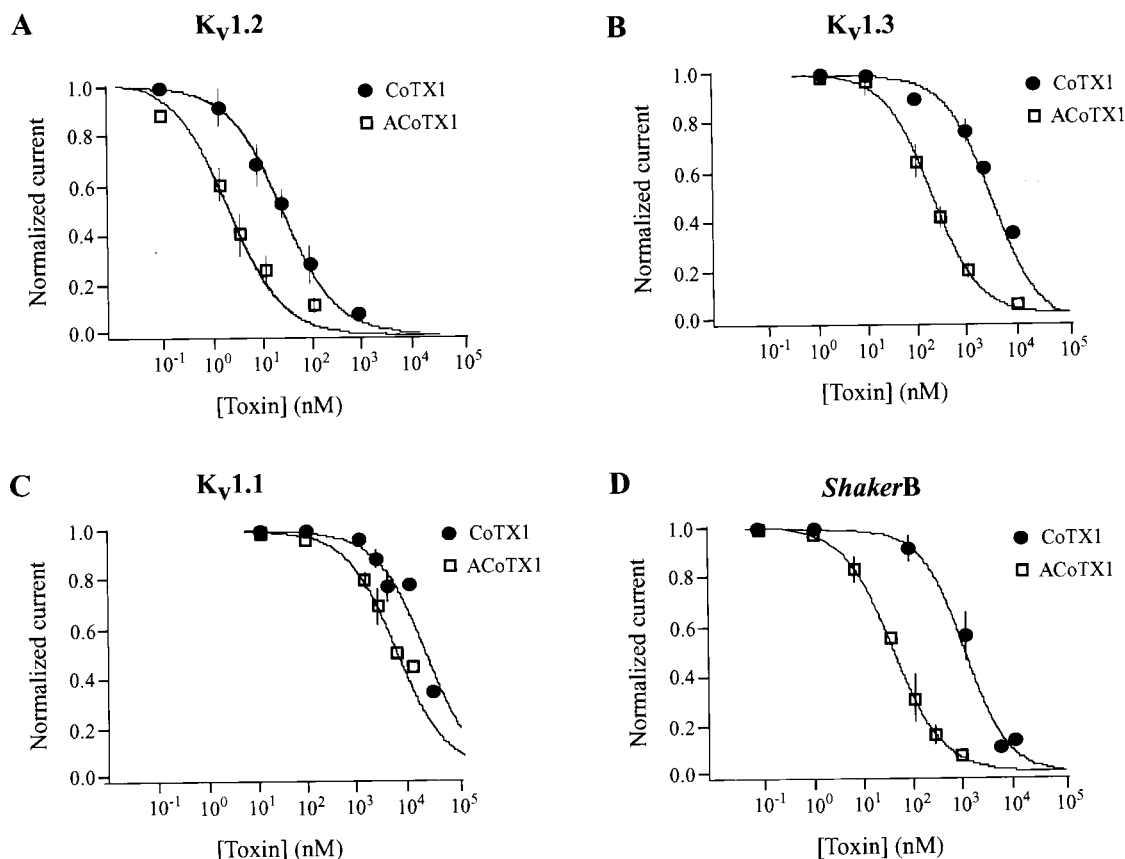
Figure 8   Blocking efficacies of CoTX1 and ACoTX1 towards voltage-gated K+ channel subtypes

(**A**) Dose–response curves for rat $K_v1.2$ K+ current inhibition by CoTX1 (●) and ACoTX1 (□). Rat $K_v1.2$ K+ channels were expressed in mammalian cells and K+ currents recorded under the whole-cell mode of the patch clamp technique. K+ currents were obtained by 200 ms depolarization from a holding potential of −80 to 40 mV. The data were fitted by a modified Hill equation as shown in the legend to Figure 7, revealing K_d values of 27 ± 4 nM for CoTX1 ($n = 20$ cells) and 1.9 ± 0.2 nM for ACoTX1 ($n = 29$ cells). (**B**) As for (**A**) but mouse $K_v1.3$ channel. The fit by the modified Hill equation provides K_d values of 5.3 ± 1.3 μM for CoTX1 ($n = 7$ cells) and 260 ± 10 nM for ACoTX1 ($n = 14$ cells). (**C**) As in (**A**) but mouse $K_v1.1$ channel. K_d values were 24.4 ± 4 μM for CoTX1 ($n = 8$ cells) and 7.4 ± 0.9 μM for ACoTX1 ($n = 10$ cells). (**D**) As in (**A**) but *Shaker* B Δ44 K+ channels expressed in rat basophilic leukaemia cells. K_d values were 1.0 ± 0.1 μM for CoTX1 ($n = 7$ cells) and 88 ± 23 nM for ACoTX1 ($n = 15$ cells).

Both peptides were also evaluated on human $K_v1.5$ and mouse $K_v3.1$ channels and were found to be inactive at concentrations in the micromolar range. Two points should be noted from the pharmacological data. First, ACoTX1 was designed to introduce the RXCQ motif in CoTX1, which supposedly should improve its affinity for SKCa channels. This was not the case, suggesting that the motif is not sufficient *per se* to improve the affinity of the peptide for SKCa channels. Second, the two mutations introduced in ACoTX1 were chosen to affect the CoTX1 dipole moment in a way that should have decreased its activity on K_v-type K+ channels [11]. The opposite result was obtained, suggesting that charge anisotropy of CoTX1 is unlikely to be key for its bioactivity on K+ channels.

Docking of CoTX1 on to rat $K_v1.2$ channel

To examine the interaction between CoTX1 and r$K_v1.2$ at the molecular level, we generated a model of $K_v1.2$ to allow a docking simulation of CoTX1 on this channel. $K_v1.2$ was selected for docking simulations over other K+ channels because of its high-affinity interaction with CoTX1.

We first performed a Blastp (version 2.2.5; http://us.expasy.org/tools/blast/) search against the whole Protein Data Bank, to select

the correct template to generate a model of the r$K_v1.2$ channel (S5-H5-S6 region). The KcsA [23] and KvAP [37] primary structures (Swiss-Prot codes 1BL8 and 1ORS) showed the best E-Value scores for r$K_v1.2$. Similar models of $K_v1.2$ were obtained using either KcsA or KvAP as a template. In the following description of the results, we exclusively report data generated with KcsA as template. The 3-D structure of CoTX1 in solution, described herein, and the molecular model of ACoTX1, were used in docking experiments with the r$K_v1.2$ model (S5-H5-S6 region) generated according to the procedures described in the Materials and methods section. Figure 9 illustrates the result of the docking simulation between CoTx1 and r$K_v1.2$. According to the docking model, the CoTX1–$K_v1.2$ complex is stabilized by four salt bridges between the side chains of three Asp[355] and one Asp[363] from distinct r$K_v1.2$ α-subunits ($K_v1.2$ channel is composed of four α-subunits) and Arg[6] or Lys[10], Arg[14], Lys[28] and Arg[18] of CoTX1, respectively. These four or five CoTX1 amino acid residues form a ring of basic residues. The Lys[21] side chain of CoTX1 enters into the ion-channel pore and is surrounded by the four Asp[379] carbonyl oxygen atoms of the P-domain selectivity filter. Residue Tyr[30] of CoTX1 is in contact with a hydrophobic cluster of aromatic residues consisting of Trp[366], Trp[367] and Tyr[377] (all located on the same $K_v1.2$ α-subunit). By
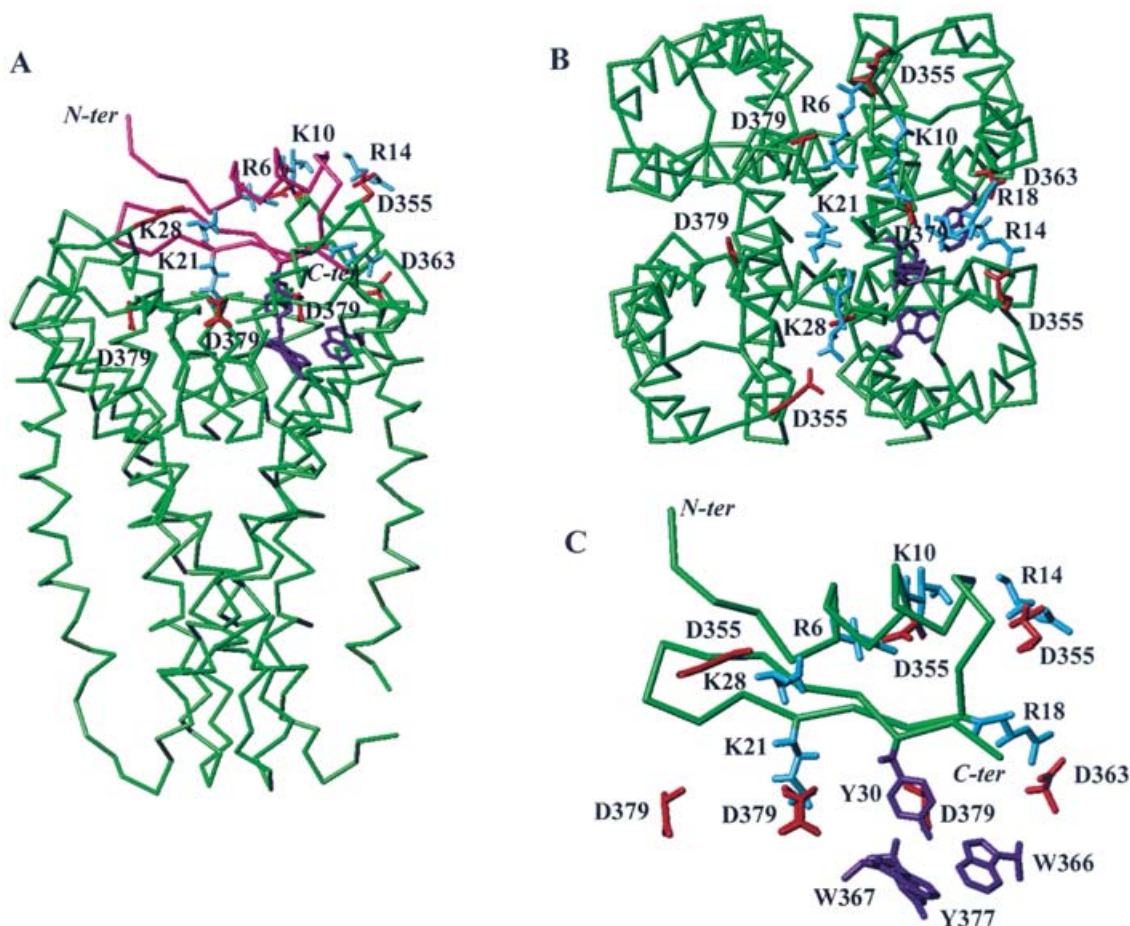
Figure 9   Docking of CoTX1 on to rat $K_v1.2$ channels (pore regions)

(**A**) Side view (Turbo-Frodo software) depicting the interaction of CoTX1 (3-D structure in solution) with rat $K_v1.2$ channels (molecular model of the pore regions) [24]. For clarity, only Cα peptide backbones of two out of the four S5-H5-S6 α-subunits of the $K_v1.2$ channels are shown (green). The Cα peptide backbone of CoTX1 is shown in pink. The side chains of amino acid residues being involved in the CoTX1–$K_v1.2$ channel interaction are detailed. Basic, acidic and aromatic residues are shown, in all panels, in light blue, red and purple, respectively. The residues are numbered according to their positions within the CoTX1 and $K_v1.2$ α-subunit amino acid sequences [1,24]. (**B**) Top view showing the docking [28] of CoTX1 on to rat $K_v1.2$ channels (pore regions). The Cα peptide backbone of CoTX1 was omitted for clarity. Only interacting residues are presented with their corresponding side-chains. The Cα peptide backbones of the four α-subunits of the $K_v1.2$ channels (S5-H5-S6 domains) are shown in green. (**C**) Magnified side view detailing the interaction of CoTX1 with the $K_v1.2$ channels. The Cα peptide backbone of CoTX1 is shown in green. For CoTX1, only the side chains of residues involved in this interaction are described. Also, only interacting residues from the $K_v1.2$ α-subunits are represented in their exact 3-D positions, according to the ion channel molecular model.

comparison with other K_v-acting toxins, the functional dyad of CoTX1 is probably composed of Lys[21] and Tyr[30]. We suggest a two-step pictorial view of CoTX1 binding in which the toxin ring of basic residues (ring composed of Arg[6] or Lys[10], Arg[14], Arg[18] and Lys[28]) would first play a crucial role (via electrostatic forces) in the recognition, interaction and correct positioning of CoTX1 on the $K_v1.2$ channel. Second, a tighter interaction would take place through mainly hydrophobic forces between Tyr[30] (dyad) and the aromatic cluster consisting of Trp[366], Trp[367] and Tyr[377] residues. The Lys[21] (dyad) side chain of CoTX1 would enter the ion channel pore to block K$^+$ efflux.

Similar docking analyses based on models of $K_v1.1$ and $K_v1.3$ did not give good scores for CoTX1, in agreement with its poor bioactivity on these channels. In contrast, results from the docking simulation of the ACoTX1 model on $K_v1.2$ reveal an identical positioning of the peptide over the channel. It should be noted that in the ACoTX1 primary structure, the two residue substitutions (Pro[7] and Gln[9]), as compared with its native counterpart, are located close to two out of the five potentially important residues

of the basic ring (Arg[6] and Lys[10]). The presence of a negative charge on the side chain of Asp[9] in CoTX1 may weaken the interaction between Lys[10] of CoTX1 and Asp[355] of Kv1.2. The substitution of Asp[9] by an uncharged Gln residue in ACoTX1 may, on the contrary, reinforce this interaction. Such an alteration in electrostatic properties could provide a reasonable explanation regarding the increased affinity of ACoTX1 for K_v-type channels.

Concluding remarks

In the present work, we describe for the first time the chemical synthesis, disulphide bridge organization, 3-D solution structure and docking results of CoTX1, a member of a novel class of α-KTx toxins. CoTX1, which is folded according to a α/β-scaffold, is the first toxin cross-linked by three disulphide bridges that is shown to be active on both voltage-gated ($K_v1.2$) and calcium-activated (IKCa1) K$^+$ channels. Our work extends a

previous study made by Selisko and co-workers in defining the pharmacological targets of CoTX1 [1]. It was shown by these authors that CoTX1 inhibits *Shaker* B and mouse Kv1.1 channels. It will be of interest to evaluate the effects of CoTX1 on a still wider range of potential pharmacological targets in future experiments, including channels with different ionic selectivity. With regard to the current targets, it is clear that docking experiments will be helpful to guide the design of more potent and/or selective CoTX1 structural analogues. In this respect, ACoTX1 already appears to be a higher-affinity blocker for several K^+ channels tested here (K_v1.2, K_v1.3, *Shaker* B Δ44 and IKCa1). From the use of this analogue, we conclude that charge anisotropy does not appear to be a relevant factor in ion-channel recognition and blockage. Further experimental data will be required to evaluate whether the dipole moments of other scorpion toxins have a role in the properties of these toxins.

REFERENCES

1 Selisko, B., Garcia, C., Becerril, B., Gomez-Lagunas, F., Garay, C. and Possani, L. (1998) Cobatoxins 1 and 2 from *Centruroides noxius* Hoffmann constitute a subfamily of potassium-channel-blocking scorpion toxins. Eur. J. Biochem. **254**, 468–479

2 Miller, C. (1995) The charybdotoxin family of K^+ channel-blocking peptides. Neuron **15**, 5–10

3 Bontems, F., Roumestand, C., Gilquin, B., Ménez, A. and Toma, F. (1991) Refined structure of charybdotoxin: common motifs in scorpion toxins and insect defensins. Science **254**, 1521–1523

4 Olamendi-Portugal, T., Gomez-Lagunas, F., Gurrola, G. B. and Possani, L. D. (1996) A novel structural class of K^+-channel blocking toxin from the scorpion *Pandinus imperator*. Biochem. J. **315**, 977–981

5 Rogowski, R. S., Collins, J. H., O'Neill, T. J., Gustafson, T. A., Werkman, T. R., Rogowski, R. A., Tenenholz, T. C., Weber, D. J. and Blaustein, M. P. (1996) Three new toxins from the scorpion *Pandinus imperator* selectively block certain voltage-gated K^+ channels. Mol. Pharmacol. **50**, 1167–1177

6 Fajloun, Z., Carlier, E., Lecomte, C., Geib, S., di Luccio, E., Bichet, D., Mabrouk, K., Rochat, H., De Waard, M. and Sabatier, J. M. (2000) Chemical synthesis and characterization of Pi1, a scorpion toxin from Pandinus imperator active on K^+ channels. Eur. J. Biochem. **267**, 5149–5155

7 Vincent, J. P., Schweitz, H. and Lazdunski, M. (1975) Structure-function relationships and site of action of apamin, a neurotoxic polypeptide of bee venom with an action on the central nervous system. Biochemistry **14**, 2521–2525

8 Chicchi, G. G., Gimenez-Gallego, G., Ber, E., Garcia, M. L., Winquist, R. and Cascieri, M. (1988) Purification and characterization of a unique potent inhibitor of apamin binding from the *Leiurus quinquestriatus hebraeus* venom. J. Biol. Chem. **263**, 10192–10197

9 Sabatier, J. M., Zerrouk, H., Darbon, H., Mabrouk, K., Benslimane, A., Rochat, H., Martin-Eauclaire, M. F. and Van Rietschoten, J. (1993) P05, a new leiurotoxin 1-like scorpion toxin: synthesis and structure-activity relationships of the α-amidated analog, a ligand of Ca^{2+}-activated K^+ channels with increased affinity. Biochemistry **32**, 2763–2770

10 Lecomte, C., Ferrat, G., Fajloun, Z., Van Rietschoten, J., Rochat, H., Martin-Eauclaire, M. F., Darbon, H. and Sabatier, J. M. (1999) Chemical synthesis and structure-activity relationships of Ts κ, a novel scorpion toxin acting on apamin-sensitive SKCa channel. J. Pept. Res. **54**, 369–376

11 Blanc, E., Sabatier, J. M., Kharrat, R., Meunier, S., El Ayeb, M., Van Rietschoten, J. and Darbon, H. (1997) Solution structure of maurotoxin, a scorpion toxin from *Scorpio maurus*, with high affinity for voltage-gated potassium channels. Proteins **29**, 321–333

12 Merrifield, R. B. (1986) Solid-phase peptide synthesis. Science **232**, 341–347

13 Mosbah, A., Kharrat, R., Fajloun, Z., Renisio, J. G., Blanc, E., Sabatier, J. M., El Ayeb, M. and Darbon, H. (2000) A new fold in the scorpion toxin family, associated with an activity on a ryanodine-sensitive calcium channel. Proteins **40**, 436–442

14 Marion, D. and Wüthrich, K. (1983) Application of phase sensitive two-dimensional correlated spectroscopy (COSY) for measurements of ^{1}H-^{1}H spin-spin coupling constants in proteins. Biochem. Biophys. Res. Commun. **113**, 967–974

15 Piotto, M., Saudek, V. and Sklenar, V. (1992) Gradient-tailored excitation for single-quantum NMR spectroscopy of aqueous solutions. J. Biomol. NMR **2**, 661–665

16 Wüthrich, K. (ed.) (1986) in NMR of Proteins and Nucleic Acids, pp. 117–176, John Wiley and Sons, New York

17 Bartels, C., Xia, T.-H., Billeter, M., Güntert, P. and Wüthrich, K. (1995) The program XEASY for computer-supported NMR spectral analysis of biological macromolecules. J. Biomol. NMR **5**, 1–10

18 Güntert, P., Braun, W. and Wüthrich, K. (1991) Efficient computation of three-dimensional protein structures in solution from NMR data using the programs CALIBA, HABAS and GLOMSA. J. Mol. Biol. **217**, 517–530

19 Güntert, P. and Wüthrich, K. (1991) Improved efficiency of protein structure calculations from NMR data using the program DIANA with redundant dihedral angle constraints. J. Biomol. NMR, **1**, 447–456

20 Mosbah, A., Belaïch, A., Bornet, A., Belaïch, J. P., Henrissat, B. and Darbon, H. (2000) Solution structure of the module X2_1 of unknown function of the cellulosomal scaffolding protein CipC of *Clostridium cellulolyticum*. J. Mol. Biol. **304**, 201–217

21 Roussel, A. and Cambillau, C. (1989) Silicon Graphics Geometry Partner Directory, pp. 77–78, Silicon Graphics, Mountain View, CA

22 Laskowski, R. A., MacArthur, M. W., Moss, D. S., and Thornton, J. M. (1993) A program to check the stereochemical quality of protein structures. J. Appl. Crystallogr. **26**, 283–291

23 Morais-Cabral, J. H., Lee, A., Cohen, S. L., Chait, B. T., Li, M. and Mackinnon, R. (1998) The structure of the potassium channel: molecular basis of K^+ conduction and selectivity. Science **280**, 69–77

24 Christie, M. J. (1995) Molecular and functional diversity of K^+ channels. Clin. Exp. Pharmacol. Physiol. **22**, 944–951

25 Brünger, A. T., Adams, P. D., Clore, G. M., DeLano, W. L., Gros, P., Grosse-Kunstleve, R. W., Jiang, J. S., Kuszewski, J., Nilges, M., Pannu, N. S. et al. (1998) Crystallography and NMR system (CNS): a new software system for macromolecular structure determination. Acta Crystallogr. **54**, 905–921

26 Nicholls, A., Sharp, K. A. and Honig, B. (1991) Protein folding and association: insights from the interfacial and thermodynamic properties of hydrocarbons. Proteins **11**, 281–296

27 Nicholls, A. and Honig, B. (1991) A rapid finite difference algorithm, utilizing successive over-relaxation to solve the Poisson-Boltzmann equation. J. Comp. Chem. **12**, 435–445

28 Palma, P. N., Krippahl, L., Wampler, J. E. and Moura, J. J. (2000) BiGGER: a new (soft) docking algorithm for predicting protein interactions. Proteins **39**, 372–384

29 Darbon, H., Blanc, E. and Sabatier, J. M. (1999) Three-dimensional structure of scorpion toxins: towards a new model of interaction with potassium channels. In Perspectives in Drug Discovery and Design: Animal Toxins and Potassium Channels, vols 15/16 (Darbon, H. and Sabatier, J. M., eds.), pp. 41–60, Kluwer Academic Publishers, Dordrecht

30 Gray, E. G. and Whittaker, V. P. (1962) The isolation of nerve endings from brain: an electron microscopic study of cell fragments derived by homogenization centrifugation. J. Anat. **96**, 79–88

31 Grissmer, S., Nguyen, A. N., Aiyar, J., Hanson, D. C., Mather, R. J., Gutman, G. A., Karmilowicz, M. J., Auperin, A. A. and Chandy, K. G. (1994) Pharmacological characterization of five cloned voltage-gated K^+ channels, types Kv 1.1, 1.2, 1.3, 1.5, and 3.1, stably expressed in mammalian cell lines. Mol. Pharmacol. **45**, 1227–1234

32 Hamill, O. P., Marty, A., Neher, E., Sakmann, B. and Sigworth, F. J. (1981) Improved patch-clamp techniques for high-resolution current recording from cells and cell-free membrane patches. Pflügers Arch. **391**, 85–100

33 Rauer, H. and Grissmer, S. (1996) Evidence for an internal phenylalkylamine action on the voltage-gated potassium channel Kv1.3. Mol. Pharmacol. **50**, 1625–1634

34 Johnson, W. C. (1985) Circular dichroism and its empirical application to biopolymers. Methods Biochem. Anal. **31**, 61–163

35 Ishii, T. M., Silvia, C., Hirschberg, B., Bond, C. T., Adelman, J. P. and Maylie, J. (1997) A human intermediate conductance calcium-activated potassium channel. Proc. Natl. Acad. Sci. U.S.A. **94**, 11651–11656

36 Logsdon, N. J., Kang, J., Togo, J. A., Christian, E. P. and Aiyar, J. (1997) A novel gene, hKCa4 encodes the calcium-activated potassium channel in human T lymphocytes. J. Biol. Chem. **272**, 32723–32726

37 Jiang, Y., Lee, A., Chen, J., Ruta, V., Cadene, M., Chait, B. T. and MacKinnon, R. (2003) X-ray structure of a voltag-dependent K^+ channel. Nature (London) **423**, 33–41

38 Gimenez-Gallejo, G., Navia, M. A., Reuben, J. P., Katz, G. M., Kaczorowski, G. J. and Garcia, M. L. (1988) Purification, sequence, and model structure of charybdotoxin, a potent selective inhibitor of calcium-activated potassium channels. Proc. Natl. Acad. Sci. U.S.A. **85**, 3329–3333

39 Carbone, E., Wanke, E., Prestipino, G., Possani, L. D. and Maelicke, A. (1982) Selective blockage of voltage-dependent K^+ channels by a novel scorpion toxin. Nature (London) **296**, 90–101

40 Crest, M., Jacquet, G., Gola, M., Zerrouk, H., Benslimane, A., Rochat, H., Mansuelle, P. and Martin-Eauclaire, M. F. (1992) Kaliotoxin, a novel peptidyl inhibitor of neuronal BK-type Ca^{2+}-activated K$^+$ channels characterized from *Androctonus mauretanicus mauretanicus* venom. J. Biol. Chem. **267**, 1640–1647

41 Rogowski, R. S., Krueger, B. K., Collins, J. H. and Blaustein, M. P. (1994) Tityustoxin Kα blocks voltage-gated non-inactivating K$^+$ channels and unblocks inactivating K$^+$ channels blocked by α-dendrotoxin in synaptosomes. Proc. Natl. Acad. Sci. U.S.A. **91**, 1475–1479

42 Gomez-Lagunas, F., Olamendi-Portugal, T., Zamudio, F. Z. and Possani, L. D. (1996) Two novel toxins from the venom of the scorpion *Pandinus imperator* show that the N-terminal amino acid sequence is important for their affinities towards *Shaker* B K$^+$ channels. J. Membr. Biol. **152**, 49–56

43 Zerrouk, H., Laraba-Djebari, F., Fremont, V., Meki, A., Darbon, H., Mansuelle, P., Oughideni, R., Van Rietschoten, J., Rochat, H. and Martin-Eauclaire, M. F. (1996) Characterization of PO1, a new peptide ligand of the apamin-sensitive Ca^{2+}-activated K$^+$ channel. Int. J. Pept. Prot. Res. **48**, 514–521